

---

Title	Coded aperture imaging of fusion source in a plasma focus operated with pure D <sub>2</sub> and a D <sub>2</sub> -Kr gas admixture
Author(s)	S. V. Springham, A. Talebitaher, P. M. E. Shutler, S. Lee, R. S. Rawat and P. Lee
Source	<i>Applied Physics Letters</i> , 101(11): 114104. doi: 10.1063/1.4752256
Published by	American Institute of Physics

---

© 2012 American Institute of Physics. This article may be downloaded for personal use only. Any other use requires prior permission of the authors and the American Institute of Physics.

The following article appeared in Springham, S. V., Talebitaher, A., Shutler, P. M. E., Lee, S., Rawat, R. S., & Lee, P. (2012). Coded aperture imaging of fusion source in a plasma focus operated with pure D<sub>2</sub> and a D<sub>2</sub>-Kr gas admixture. *Applied Physics Letters*, 101(11), 114104. doi: 10.1063/1.4752256 and may be found at <http://dx.doi.org/10.1063/1.4752256>

## Coded aperture imaging of fusion source in a plasma focus operated with pure D2 and a D2-Kr gas admixture

S. V. Springham, A. Talebitaher, P. M. E. Shutler, S. Lee, R. S. Rawat et al.

Citation: *Appl. Phys. Lett.* **101**, 114104 (2012); doi: 10.1063/1.4752256

View online: <http://dx.doi.org/10.1063/1.4752256>

View Table of Contents: <http://apl.aip.org/resource/1/APPLAB/v101/i11>

Published by the [American Institute of Physics](#).

---

### Related Articles

Experimental evidence of foam homogenization

*Phys. Plasmas* **19**, 113105 (2012)

Three-dimensional modeling of beam emission spectroscopy measurements in fusion plasmas

*Rev. Sci. Instrum.* **83**, 113501 (2012)

Dynamics of femto- and nanosecond laser ablation plumes investigated using optical emission spectroscopy

*J. Appl. Phys.* **112**, 093303 (2012)

Orientation phenomena for the  $1s \rightarrow 2p \pm 1$  atomic collisional excitations in quantum plasmas: Shielding and plasmon coupling

*Phys. Plasmas* **19**, 113301 (2012)

Laser schlieren deflectometry for temperature analysis of filamentary non-thermal atmospheric pressure plasma

*Rev. Sci. Instrum.* **83**, 103506 (2012)

---

### Additional information on *Appl. Phys. Lett.*

Journal Homepage: <http://apl.aip.org/>

Journal Information: [http://apl.aip.org/about/about\\_the\\_journal](http://apl.aip.org/about/about_the_journal)

Top downloads: [http://apl.aip.org/features/most\\_downloaded](http://apl.aip.org/features/most_downloaded)

Information for Authors: <http://apl.aip.org/authors>

## ADVERTISEMENT



**Goodfellow**  
metals • ceramics • polymers • composites  
70,000 products  
450 different materials  
small quantities fast

[www.goodfellowusa.com](http://www.goodfellowusa.com)

## Coded aperture imaging of fusion source in a plasma focus operated with pure $D_2$ and a $D_2$ -Kr gas admixture

S. V. Springham,<sup>1</sup> A. Talebitaher,<sup>1</sup> P. M. E. Shutler,<sup>1</sup> S. Lee,<sup>1,2</sup> R. S. Rawat,<sup>1</sup> and P. Lee<sup>1</sup>

<sup>1</sup>National Institute of Education, Nanyang Technological University, 1 Nanyang Walk, 637616 Singapore

<sup>2</sup>Institute for Plasma Focus Studies, 32 Oakpark Drive, Chadstone VIC3148, Australia

(Received 12 June 2012; accepted 27 August 2012; published online 11 September 2012)

The coded aperture imaging (CAI) technique has been used to investigate the spatial distribution of DD fusion in a 1.6 kJ plasma focus (PF) device operated in, alternatively, pure deuterium or deuterium-krypton admixture. The coded mask pattern is based on a singer cyclic difference set with 25% open fraction and positioned close to  $90^\circ$  to the plasma focus axis, with CR-39 detectors used to register tracks of protons from the  $D(d,p)T$  reaction. Comparing the coded aperture imaging proton images for pure  $D_2$  and  $D_2$ -Kr admixture operation reveals clear differences in size, density, and shape between the fusion sources for these two cases. © 2012 American Institute of Physics. [<http://dx.doi.org/10.1063/1.4752256>]

Investigation of the detailed nature of deuterium-deuterium (DD) fusion in the plasma focus (PF) remains one of the most challenging aspects of PF research. Considerable overall support for beam-target models of PF fusion derives from their compatibility with experimental measurements<sup>1–3</sup> of neutron yield, anisotropy, energy (from time-of-flight), and emission duration. However, details of the mechanisms responsible for deuteron acceleration, the distributions of deuteron energies and directions, the role of magnetic gyration, and the spatial extent of the fusion source are still poorly understood. Fusion source imaging is a strong approach which can help to confirm or reject various PF fusion models. However, due to the penetrating nature of fast neutrons and the relatively small dimensions of the fusion source, it is extremely difficult to arrange a satisfactory scheme for pinhole/collimation imaging of the neutron emission. On the other hand, it is fairly easy to make a satisfactory pinhole for the  $\sim 3$  MeV fusion protons. And since the two fusion reactions  $D(d,p)T$  and  $D(d,n)^3He$  occur with almost equal probabilities, the neutron and proton yields per shot are very similar. Furthermore, comparing the fusion proton images for each PF shot with its corresponding x-ray image (which shows the hottest and densest plasma regions) should highlight any contributions from thermonuclear fusion within the pinch.

Jäger *et al.*<sup>4</sup> have reported one of the few experiments in which DD fusion proton imaging was performed on a PF device. These measurements were carried out on the large machine, POSEIDON,<sup>5</sup> with a stored energy of 280 kJ and a correspondingly high neutron/proton yield of  $\sim 10^{11}$  per shot. They obtained good precision proton images using a pinhole covering a solid-angle of  $1.46 \times 10^{-4}$  sr. However, single pinhole proton imaging is much less feasible for small PF devices (i.e., below about 5 kJ stored energy) due to the low number of proton tracks recorded. To overcome this limitation and obtain bright fusion source images for the 1.6 kJ NX2 device,<sup>6</sup> we have employed the coded aperture imaging (CAI) technique using mask patterns based on singer cyclic difference sets<sup>7</sup> (CDS). Fusion images were obtained for single PF shots with neutron yields in the range  $1–3 \times 10^8$

Singer set patterns permit the mask open fraction to be selected so as to obtain a near optimum signal-to-noise ratio (SNR) for a source of a given spatial extent.<sup>8</sup> For the experiments, we report in Ref. 6, the  $20 \times 20$  pixel mask had 57 square holes of  $400 \mu\text{m}$  side, giving a total open area of  $\sim 9 \text{ mm}^2$  and a position resolution of  $\sim 1 \text{ mm}$ . A hollow anode was used for those measurements, which necessitated placing the CAI cameras at  $45^\circ$  forward viewing angles so as to obtain an unobscured view of the pinch column (approximately half of which lay “inside” the hollow anode). The depth-of-field problem and lack of space to increase mask area are disadvantages of this oblique viewing arrangement.

To obtain brighter proton images with better resolution, a larger mask has been designed with 341 square holes of  $300 \mu\text{m}$  side, giving a total open area of  $30.69 \text{ mm}^2$ . The hollow PF anode was replaced with a conically tipped anode (see Fig. 1) and the CAI camera was positioned close to the

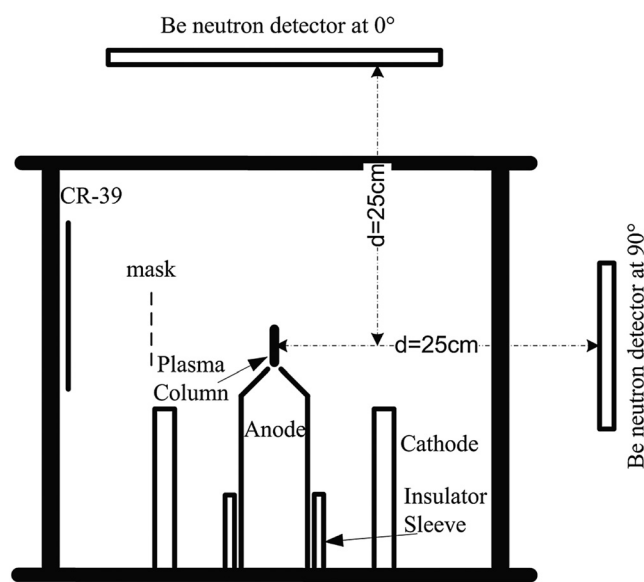


FIG. 1. Schematic of experimental setup showing: NX2 plasma focus, CAI mask, CR-39 detector, and two beryllium neutron activation counters (positioned axially and radially). The x-ray pinhole imaging system is not shown.

PF radial direction, so that the whole pinch could be imaged. The  $91 \times 15$  mask pattern used is based on a Singer CDS with  $p = 1365$  pixels and  $h = 341$  holes (open fraction of  $\rho = 0.25$ ). The mask pattern rows (oriented perpendicular to the  $z$ -axis) were spaced by a factor of 6 to increase the image SNR and avoid excessive overlap of proton tracks on the surface of the CR-39 detectors. By convention, the positive  $z$  (or downstream) direction is parallel to and away from the anode. The overall dimensions of the mask are then almost square:  $27.3(\text{horiz}) \times 25.5(\text{vert}) \text{ mm}^2$ . The mask was fabricated by laser-drilling square holes of  $300 \mu\text{m}$  side in  $50 \mu\text{m}$  stainless steel foil using an Avia-X Q-switched third-harmonic Nd:YVO<sub>4</sub> diode-pumped laser.

CR-39 nuclear track detectors (Intercast Europe Srl, Parma, Italy) were employed to register the DD fusion protons. A  $75 \mu\text{m}$  thick Kapton film was placed immediately in front of the CR-39 detectors to stop all energetic charged particles (mostly deuterons) other than the  $\sim 3 \text{ MeV}$  protons. The CAI camera system was located inside the NX2 vacuum chamber close to the radial PF direction. As shown in Fig. 1, the lowest row of mask holes was level with the anode-tip. The source-to-mask and mask-to-detector distances were  $d_1 = 44 \text{ mm}$  and  $d_2 = 40 \text{ mm}$ , respectively, giving an open solid angle of  $1.32 \times 10^{-2} \text{ sr}$ . The dimensions of the CR-39 detectors used were  $67(\text{horiz}) \times 77(\text{vert}) \text{ mm}^2$  giving a fully coded field of view<sup>6</sup> (FOV) in the source plane of  $2.8 \times 1.7 \text{ cm}^2$ . Hence, the anticipated  $\sim 1.0 \times 0.3 \text{ cm}^2$  fusion source of the NX2 lies easily within this FOV. The resolution of CAI camera (i.e., the magnified pixel size in the source plane) for this geometry is  $0.63 \text{ mm}$ . The internal angle of the conical anode tip is  $130^\circ$ , and the coded mask spans the angular range  $60^\circ$  to  $90^\circ$  relative to the PF axis. The pinch current for good shots was close to  $300 \text{ kA}$ , and hence the deflection of proton trajectories in the magnetic field around the dense plasma column was analogous to that described in Ref. 6. The anode cone-angle and CAI camera position were chosen based on these proton trajectory calculations to ensure that protons emitted from the upstream end of the pinch column could reach the CAI camera unobstructed.

An x-ray pinhole camera was employed to record the time-integrated image of the hot ( $\sim \text{keV}$ ) plasma x-ray source for each shot. It comprised a  $1/3 \text{ in.}$  CCD sensor with  $768 \times 576$  pixels, and a laser-drilled pinhole through  $50 \mu\text{m}$  thick tungsten foil. The demagnification for this pinhole camera was 4.5. For pure deuterium operation, the pinhole was covered with a  $20 \mu\text{m}$  Be filter to cut all photons with energies below  $\sim 700 \text{ eV}$ . For deuterium-krypton operation, a  $12.5 \mu\text{m}$  Ti plus  $50 \mu\text{m}$  Be filter combination was used. Both sets of filters transmit the Cu  $K_\alpha$  and  $K_\beta$  x-rays of energies  $\sim 8$  and  $8.9 \text{ keV}$ , which permits the position of the copper anode tip to be observed in many of the x-ray images.

To measure the time-integrated neutron yield and anisotropy, two beryllium fast-neutron activation counters<sup>9</sup> were positioned  $25 \text{ cm}$  from the anode tip in the axial and radial directions, respectively. A plastic scintillation detector, positioned  $3 \text{ m}$  from the PF anode in the radial direction, measured the time-resolved neutron emission; a  $5 \text{ cm}$  thick lead block placed in front of this detector strongly attenuated the hard x-ray radiation emitted during the PF discharge. To measure the time-resolved hard x-ray emission two more

scintillation detectors, cesium-iodide (CsI:pure) and barium-fluoride (BaF<sub>2</sub>), were positioned adjacent to the plastic scintillation detector but without the Pb-shielding. These two crystals have short scintillation decay times: CsI:pure  $15 \text{ ns}$  and BaF<sub>2</sub>  $0.6 \text{ ns}$  (fast component). However, BaF<sub>2</sub> also has a slow component with a decay time of  $630 \text{ ns}$  and considerably higher light yield than the fast component. Therefore, for the hard x-ray pulse, the BaF<sub>2</sub> signal is useful mainly for observing its rise-time, while the CsI signal gives a measure of its duration and integrated energy.

For the pure D<sub>2</sub> series of shots, the NX2 plasma focus was operated in its neutron yield optimized regime:  $13 \text{ mbar}$ ,  $11 \text{ kV}/1.6 \text{ kJ}$ . Several CR-39 detectors were exposed to single PF shots: these being the first shot fired after evacuating the chamber and filling with deuterium gas, so that there should be no significant effect from the gas impurities, which usually accumulate over a series of shots. In spite of different neutron yields and anisotropies, the fusion source images showed quite similar spatial distributions. We have selected one “good shot” (1365-I23-A) as an example. This shot had a high neutron yield of  $3.2 \times 10^8$ , but in other respects is fairly typical of the results obtained. The high neutron anisotropy of 2.4 indicates a high average energy for deuterons producing fusion via the beam-target interaction. For this shot, Fig. 2-right shows a cone-shaped fusion source of  $\sim 11 \text{ mm}$  length. The source width is  $\sim 2 \text{ mm}$  near the anode, and widens to  $\sim 5 \text{ mm}$  near the top of the cone, with the highest fusion density occurring at  $z = 3 \text{ mm}$ . The high SNR value of 21.8 for this image is a consequence of the high number of proton tracks ( $\sim 174\,000$ ) recorded on the CR-39 detector. The corresponding x-ray image, Fig. 2-left, shows a hot dense pinch region (of  $\sim 4 \text{ mm}$  length and  $\sim 0.5 \text{ mm}$  width) above the anode tip. It also shows considerable x-ray emission from the copper anode tip due to bombardment by the energetic electron beam emitted from the pinch.

Comparison of the x-ray and fusion proton images indicates that the zone with the highest concentration of DD fusion occurs close to the downstream end of the hot dense plasma column. This can be understood in terms of deuterons being accelerated (predominantly in the  $+z$  direction) by the rapidly constricting magnetic field around the pinch, and so reaching their highest kinetic energies at the downstream end of the pinch column, where they produce fusion

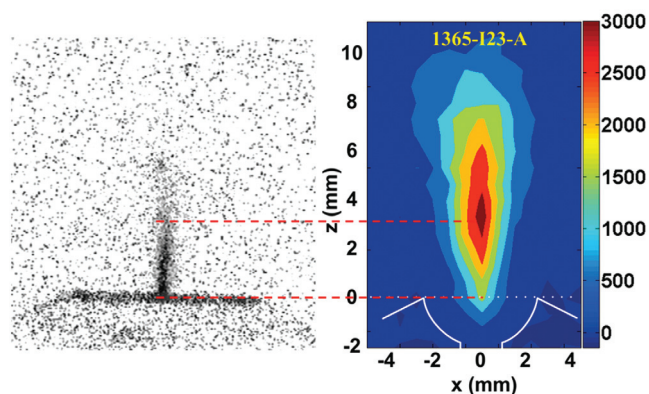


FIG. 2. Proton CAI fusion source image (right) and x-ray image (left) for pure D<sub>2</sub> gas operation (shot 1365-I23-A).

reactions with the approximately stationary and relatively high density deuterium gas within the “fountain” at this end of the pinch. This cone-shaped fusion zone at the end of the pinch column is consistent with the more extended conical distribution of fusion, due to forwardly directed deuteron beams, observed in another plasma focus device.<sup>10</sup> Of course, there is also a concentration of fusion production along the length of the pinch column (where the ion density is at its highest) before the accelerated deuterons have attained their maximum energy.

There is no noticeable indication of  $m=0$  or  $m=1$  instabilities in these fusion source images, and they are also not observed in the corresponding x-ray images. This might be due to the rapid disruption of the plasma pinch, so the x-ray emission time was too short to show any strong hot spot in the pinch column (the term “hot spot” is conventionally used to refer to particularly dense and high temperature ( $>1$  keV) regions within the pinch column). However, it has been found that the occurrence of hot spots in the pure deuterium pinch can be highly dependent on operating pressure.<sup>18</sup> Also, it is apparent that the fusion source is more localized above the pinch column, and so there may be no correlation with column instabilities.

Another aspect of plasma focus fusion that this study helps to elucidate is the influence of high-Z noble gas admixtures (with deuterium). Enhancement of bremsstrahlung x-ray yield for admixture gas operation has been reported for experiments on several PF machines,<sup>10–13</sup> and it is claimed that this higher x-ray emission both stabilizes the pinch column and increases the plasma density through enhanced compression<sup>14</sup> as a result of the radiation cooling mechanism.<sup>15,16</sup> A secondary factor contributing to this enhanced compression is the increased thermodynamic degrees of freedom in this gas mixture due to the incomplete ionization of the Kr component, which reduces the specific heat ratio of the mixture to significantly less than  $5/3$  (the value associated with dissociated pure deuterium).<sup>16</sup> The CAI fusion source images clearly show the different size and density of the fusion emission zones for pure  $D_2$  and  $D_2$ -Kr admixture (98%  $D_2$  + 2% Kr by vol.) operation. The NX2 was operated with the same parameters as for  $D_2$  (i.e., 13 mbar, 11 kV/1.6 kJ). After firing several shots, it was apparent that the higher x-ray yield from the D-Kr plasma typically saturated the CCD sensor. So, for the  $D_2$ -Kr measurements, the  $20\ \mu\text{m}$  Be filter was replaced by a  $50\ \mu\text{m}$  Be plus  $12.5\ \mu\text{m}$  Ti filter, for which the x-ray transmittance lies predominantly in the 1.0 to 2.5 keV energy range.

The majority of fusion source images in the  $D_2$ -Kr admixture case show a similar structure. For the selected illustrative shot, 1365-I28-A, the neutron yield was  $4.1 \times 10^8$ . The relatively low neutron anisotropy of 2.17 indicates a lower average energy of beam deuterons involved in the fusion reactions. The image of fusion source in Fig. 3-right appears as a prolate ellipsoid of  $\sim 2$  mm width and  $\sim 6$  mm length, with the highest concentration of fusion near the geometrical center ( $z = 6.5$  mm). A very high SNR value of 50.8 for this image is due to the high number of proton tracks (187 000) and compact geometry of the source.

The corresponding x-ray image (Fig. 3-left) clearly shows the existence of high density hot spots possibly associ-

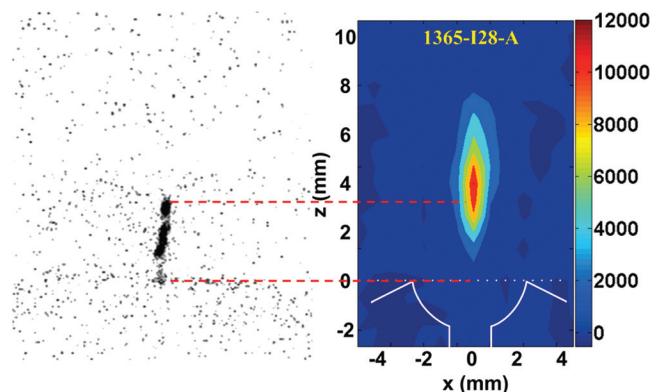


FIG. 3. Proton CAI fusion source image (right) and x-ray image (left) for  $D_2$ -Kr gas admixture operation (shot 1365-I28-A).

ated with  $m=0$  instabilities in the final compression. The pinch column length is only  $\sim 3$  mm. The hot plasma is distributed quite evenly along the  $z$ -axis. The  $m=0$  and  $m=1$  instability structures responsible for the break-up of the pinch column are not evident in the fusion source images, which indicate that the deuterons are accelerated along the pinch column and react mostly above the pinch.

In conclusion, this paper reports the implementation of the coded aperture imaging technique for fusion source imaging in the plasma focus device. We have obtained good-resolution time-integrated bright images of the DD fusion source for single shots in a 1.6 kJ plasma focus device operated in pure deuterium or a deuterium-krypton gas admixture.

The fusion source in pure deuterium appears cone-shaped, narrower near the anode, and wider at the top, but most concentrated in the central region of the pinch. There is no evidence for the existence of hot spots or  $m=0$  instabilities in the fusion source image or even in the pinch x-ray region. The observed neutron anisotropy values ( $>2.0$ ) together with the lack of axial structure in the fusion proton images are a strong indication that beam-target fusion is distributed along the length of the pinch column, and to a lesser extent, within the fountain-shaped region of high gas density at the downstream end of the column. The lack of spatial correlation between the regions of fusion and x-ray emissions for the  $D_2$ -Kr shots shows that any contribution from thermonuclear fusion is relatively small. Moreover, the downstream displacement of the fusion source relative to the x-ray source shows that, although it is not associated with  $m=0$  instabilities or micropinches, the zone of deuteron acceleration is quite compact and located within the x-ray emitting region. The model of plasma focus fusion most consistent with our observations is that based on ion (deuteron) acceleration within a plasma diode,<sup>17</sup> which results from anomalous resistivity in the pinch.

In contrast to the pure deuterium case, Kr-doped operation produces a prolate ellipsoidal fusion source, which is smaller and more concentrated in the centre. The x-ray images clearly show the existence of hot spots/micropinches in the final compression phase, and the resultant radiation cooling leads to this compact highly compressed plasma pinch.

- <sup>1</sup>A. Mozer, M. Sadowski, H. Herold, and H. Schmidt, *J. Appl. Phys.* **53**, 2959 (1982).
- <sup>2</sup>R. L. Gullickson and H. L. Sahlin, *J. Appl. Phys.* **49**, 1099 (1978).
- <sup>3</sup>H. Krompholz, L. Michel, K. H. Schonbach, and H. Fischer, *Appl. Phys.* **13**, 29 (1977).
- <sup>4</sup>U. Jäger, L. Bertalot, and H. Herold, *Rev. Sci. Instrum.* **56**, 77 (1985).
- <sup>5</sup>H. Herold, L. Bertalot, K. Hirano, U. Jäger, H. J. Kaeppler, M. J. Sadowski, H. Schmidt, R. Schmidt, M. Shakhatre, A. Shyam *et al.*, *Plasma Physics and Controlled Nuclear Fusion Research* (IAEA, Vienna, 1985), Vol. 2, p. 579.
- <sup>6</sup>A. Talebitaher, S. V. Springham, P. M. E. Shutler, P. Lee, and R. S. Rawat, *J. Fusion Energy* **31**, 234 (2012).
- <sup>7</sup>P. M. E. Shutler, A. R. Talebitaher, and S. V. Springham, *Nucl. Instrum. Methods Phys. Res. A* **669**, 22 (2012).
- <sup>8</sup>J. Singer, *Trans. Am. Math. Soc.* **43**, 377 (1938).
- <sup>9</sup>A. Talebitaher, S. V. Springham, R. S. Rawat, and P. Lee, *Nucl. Instrum. Methods Phys. Res. A* **659**, 361 (2011).
- <sup>10</sup>S. V. Springham, S. Lee, and S. P. Moo, *Braz. J. Phys.* **32**, 172 (2002).
- <sup>11</sup>Y. Kato and S. H. Be, *Appl. Phys. Lett.* **48**, 686 (1986).
- <sup>12</sup>P. S. Antsiferov, F. B. Rosmej, O. N. Rosmej, H. Schmidt, D. Schulz, and A. Schulz, *J. Appl. Phys.* **77**, 4973 (1995).
- <sup>13</sup>V. V. Vikhrev and S. I. Braginski, *Reviews of Plasma Physics*, edited by M. A. Leontovich (Consultants Bureau, New York, 1986), Vol. 10, p. 425.
- <sup>14</sup>R. Verma, P. Lee, S. V. Springham, T. L. Tan, R. S. Rawat, and M. Krishnan, *Appl. Phys. Lett.* **92**, 011506 (2008).
- <sup>15</sup>C. A. Coverdale, C. Deeney, A. L. Velikovich, R. W. Clark, Y. K. Chong, J. Davis, J. Chittenden, C. L. Ruiz, G. W. Cooper, A. J. Nelson, J. Franklin, P. D. LePell, J. P. Apruzese, J. Levine, J. Banister, and N. Qi, *Phys. Plasma* **14**, 022706 (2007).
- <sup>16</sup>S. Lee, S. H. Saw, and J. Ali, "Numerical experiments on radiative cooling and collapse in plasma focus operated in krypton," *J. Fusion Energy* (in press).
- <sup>17</sup>V. A. Gribkov, A. Banaszak, B. Bienkowska, A. V. Dubrovsky, I. Ivanova-Stanik, L. Jakubowski, L. Karpinski, R. A. Miklaszewski, M. Paduch, M. J. Sadowski *et al.*, *J. Phys. D: Appl. Phys.* **40**, 3592–3607 (2007).
- <sup>18</sup>M. Zakaullah, I. Akhtar, A. Waheed, K. Alamgir, A. Z. Shah, and G. Mur-taza, *Plasma Sources Sci. Technol.* **7**, 206–218 (1998).